Subsidence of THA stems due to acrylic cement creep is extremely sensitive to interface friction

Pergamon

PII: S0021-9290(96)00077-2

J. Biomechanics, Vol. 29, No. 12, pp. 1569–1575, 1996

Printed in Great Britain
0021-9290/96 $15.00 + .00

SUBSIDENCE OF THA STEMS DUE TO ACRYLIC CEMENT CREEP IS EXTREMELY SENSITIVE TO INTERFACE FRICTION

Nico Verdonschot and Rik Huiskes*

Biomechanics Section, Institute of Orthopaedics, University of Nijmegen, P.O. Box 9101, 6500 HB Nijmegen, The Netherlands

Abstract—Acrylic cement, used to fixate total hip arthroplasty (THA), creeps under dynamic and static loading conditions. As a result, THA stems which are debonded from the cement, may gradually subside, depending on their shape and surface roughness. The purpose of this study was to evaluate the relationship among dynamic load, creep characteristics, interface friction, and subsidence patterns.

A laboratory model consisting of a metal tapered cone, surrounded by a cement mantle, was developed. The cone was gradually compressed in the cement by a dynamic, sinusoidal axial force, cycling between 0 and 7 kN for 1.7 million cycles at a frequency of 1 Hz. Subsidence and cement strain were monitored. Two tapers were tested in this way. The relationships among subsidence, creep properties and interface friction were evaluated from a finite element (FE) model, used to simulate the experiments. In this model, the creep properties obtained in dynamic and static, tension and compression experiments measured earlier, were used.

The subsidence patterns of both tapers were similar, but one subsided more than the other (380 vs 630 μm). Both subsided stepwise instead of continuous, with a frequency much smaller than that of the applied load. The characteristics of the subsidence and cement-strain patterns could be reproduced by the FE model, but not with great numerical precision. The stepwise subsidence could be explained by slip–stick mechanisms at the interface starting distally and gradually working towards proximal. Variations in friction from 0.25 to 0.50 reduced the total subsidence and the step frequency by about 50%.

It was concluded that FE-models used to simulate the mechanical endurance characteristics of THA reconstructions, extended to incorporate cement creep, produce realistic results. These results showed that prosthetic subsidence under dynamic loads occurs due to cement creep. The extent of the subsidence is extremely sensitive to interface friction, hence to small variations in surface roughness and cement constitution. This may explain the relatively large variation of *in vivo* prosthetic subsidence rates reported in the literature. Copyright © 1996 Elsevier Science Ltd.

Keywords: Total hip arthroplasty; Acrylic cement; Subsidence; Creep.

INTRODUCTION

It has been suggested that cemented femoral stems in total hip arthroplasty (THA) should be designed to take advantage of the creep properties of acrylic cement (Fowler *et al.*, 1988). These authors proposed a double tapered stem which can subside within the cement mantle to accommodate the gradual creep deformation of the cement mantle. To optimize this effect, they suggested that stem–cement friction should be minimized. Hence, the stem should be as smooth as possible. However, quantitative relationships between friction and subsidence are unknown. It is also unclear to what extent cement creeps when exposed to the stress levels that typically occur in a cement mantle, and what the effects on load transfer and the endurance of the reconstruction would be. Several investigators have measured the creep properties of bone cement under static loading conditions (Chwirut, 1984; Saha and Pal, 1982; Oysæed and Ruyter, 1989; Treharne and Brown, 1975). They found that creep strains are extensive and can exceed the elastic ones. Because acrylic cement *in vivo* is loaded dynamically, we performed cyclic tensile and compressive tests to establish the relationships among creep strain, load level, and the number of loading cycles (Verdonschot and Huiskes, 1994, 1995a). As a result of these investigations, the creep behavior of acrylic cement under unidirectional static and dynamic loading conditions is now well established.

The purpose of this study was to evaluate the relationship among dynamic load, creep characteristics, interface friction, and subsidence patterns. Using laboratory experiments and finite element (FE) models, it was investigated whether prosthetic subsidence occurs due to creep of acrylic bone cement when loaded dynamically, and how it is affected by friction at the stem–cement interface.

METHODS

The experiments

Two laboratory experiments were performed with two taper–cement structures. The two straight metal tapers, identified as Taper 1 and Taper 2, were implanted in cement mantles [Fig. 1(a)]. The taper–cement composites were stored in saline at body temperature for more than one month to permit complete polymerization and water absorption in the cement, and to allow for relaxation of the residual stresses caused by the shrinkage after cement curing (Ahmed *et al.*, 1982). The cement

Received in final form 15 *March* 1996.
*Author to whom correspondence should be addressed.

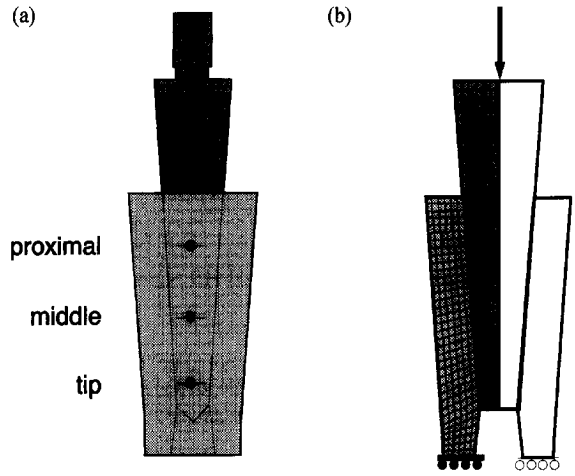

Fig. 1. (a) The tapers were implanted in a cement mantle. Three pairs of strain gauges measured the hoop strains. (b) The axisymmetric FE model of the structure. The taper–cement interface was assumed to be frictional.

mantles had a uniform thickness of 10 mm. The tapers had top angles of 8°, a distal diameter of 10 mm, and a length of 100 mm; their surfaces had been highly polished. The surface roughness were measured at four locations resulting in an average roughness value of 0.033 μm (S.D. = 0.0025) for Taper 1, and 0.039 μm (S.D. = 0.0019) for Taper 2. On the surface of each cement mantle six unidirectional strain gauges were attached, measuring the circumferential hoop strains [Fig. 1(a)]. To enhance the reliability of the strain data, gauges were mounted in pairs, one gauge at the frontal side, the other at the back side. Each gauge was incorporated in a quarter Wheatstone bridge. To be able to monitor the drift in the gauges during the experiments, two additional (dummy) gauges were attached to a small unloaded piece of acrylic cement. The strain gauges were sealed with a layer of silicon rubber and the taper was placed in a 38°C bath of saline solution. The subsidence of the tapers relative to the top of the cement mantle was measured using an extensometer with a resolution of 0.5 μm.

The tapers were exposed to compressive sinusoidal loads ranging from 0 to 7 kN at a frequency of 1 Hz for a period of 1.7 million loading cycles. During this period, the subsidence of the tapers into the cement mantles and the strain levels were monitored and stored in a computer.

The finite element simulations

The experiments were simulated using an axisymmetric FE model consisting of 270 four-node axisymmetric quadrilateral elements [Fig. 1(b)]. Young's moduli were set at 200 GPa for the taper material (stainless steel) and at 2.2 GPa for the cement material (Saha and Pal, 1984). Poisson's ratio was 0.3 for both materials. The taper–cement interface conditions were assumed to be frictional and simulated by 31 gap elements (MARC Analysis Corporation, Palo Alto, CA). The coefficient of friction was not measured but was assumed to be either 0.25 or 0.50. The former value is a realistic value for highly polished, stainless steel surfaces in contact with acrylic cement (Hampton, 1981; Mann *et al.*, 1991). The second value was chosen rather arbitrarily, to investigate the sensitivity of the creep rates on the frictional properties of the taper–cement interface.

The constitutive theory used in the creep simulation was based on the same concepts as used in the flow theory of plasticity. It was assumed that the total strain is composed of an elastic and a creep strain. The iterative procedure used in the creep simulation is depicted in Fig. 2.

The stress state in the cement mantle is three-dimensional, as determined by three principal stress components. Experimental creep data were based on uniaxial tests, which considered the presence of only one stress component (Chwirut, 1984; Verdonschot and Huiskes, 1994, 1995a). For this reason, the uniaxial creep laws could not be applied directly to structures with three-dimensional stress states. The solution for this problem was to define an equivalent stress, which relates the three-dimensional stress state to the uniaxial one, and which could be used in the creep laws. We selected the Von Mises stress as the equivalent stress, in accordance with what is usually used in creep simulations (Hinton, 1992).

Another problem which obstructed the direct use of the creep laws was the fact that they were determined assuming stress conditions which were either purely static (Chwirut, 1984), or cyclic dynamic (Verdonschot and Huiskes, 1994, 1995a). However, assuming friction at the taper–cement interface, the stress state was neither purely static, nor cyclic dynamic (Fig. 3). Due to frictional forces at the interface, stresses were not completely released after unloading. Hence, the local Von Mises stress level was divided into a residual stress and a dynamic (cyclic) one. Obviously, the Von Mises stress level at full

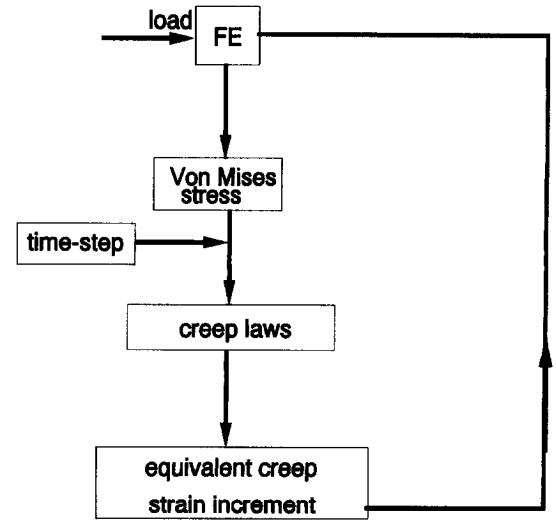

Fig. 2. The iteration scheme of the creep simulation.

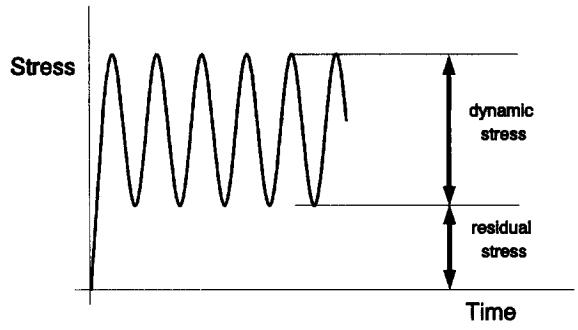

Fig. 3. Due to the frictional properties of the taper–cement interface a considerable amount of the cement mantle remains loaded even when the external load has been reduced to zero. Hence, the local loading mode of the cement can be divided into a cyclic stress amplitude, superimposed on a residual loading mode.

loading was affected by the creep process and a function of the number of loading cycles (N), according to

$$\sigma_{vm}(N) = \sigma_{dyn}(N) + \sigma_{res}(N). \quad (1)$$

The ratio (R) of the Von Mises stress levels in the cement in the unloaded and loaded situations was determined prior to the actual creep simulation by simulating one loading cycle ($N = 1$). Hence, a load of 7 kN was applied and the Von Mises stress level in every integration point was stored ($\sigma_{vm}^{loaded(N=1)}$). Subsequently, the structure was unloaded which resulted in lower values for the Von Mises stresses in the cement, but not in zero values as the taper remained stuck in the cement mantle ($\sigma_{vm}^{unloaded(N=1)}$). Consequently the ratio of the Von Mises stress level (unloaded vs loaded) was calculated at every integration point and used to identify how much of the Von Mises stress level at full loading could be considered as dynamic and how much as residual. This ratio (R) was then assumed to remain constant during the whole ensuing creep process, as described by

$$R = \frac{\sigma_{vm}^{unloaded(N=1)}}{\sigma_{vm}^{loaded(N=1)}}, \quad (2)$$

which produces

$$\sigma_{res}(N) = R\,\sigma_{vm}(N), \quad (3a)$$

and

$$\sigma_{dyn}(N) = (1 - R)\sigma_{vm}(N). \quad (3b)$$

Similar to the application of Boltzmann principle, which can be used for linear visco-elastic materials (Young and Lovell, 1991), the total creep strain was determined by superimposing the creep strain due to the residual load and that due to the dynamic loads; hence

$$\varepsilon^c(N, \sigma_{vm}, R) = \varepsilon^c_{dyn}(N, \sigma_{dyn}) + \varepsilon^c_{res}(N, \sigma_{res}). \quad (4)$$

To determine the creep strain due to the residual stress component, the creep law determined by Chwirut (1984) was used:

$$\varepsilon^c_{stat} = 1.798 \times 10^{-6} t^{0.283} \sigma_{res}^{1.858}, \quad (5)$$

where t is the loading time in seconds, and σ_{res} the residual stress level in MPa. The structure was dynamically loaded, which makes it convenient to rewrite equation (5) in terms of the number of loading cycles, instead of loading time. As a loading frequency of 1 Hz was used, the loading time (t) can simply be replaced by the number of loading cycles (N), which leads to

$$\varepsilon^c_{stat} = 1.798 \times 10^{-6} N^{0.283} \sigma_{res}^{1.858}, \quad (6)$$

where N is the number of loading cycles.

To determine the creep strain due to the dynamic stress amplitude, two creep laws are available. The first one describes the creep strain under dynamic tensile loading (Verdonschot and Huiskes, 1994), whereas the second one was established for dynamic compressive loading conditions (Verdonschot and Huiskes, 1995a). The creep strains due to the dynamic stress amplitude were calculated using one of these laws, depending on whether the local maximal principal stress (σ_{prmax}) was tensile or compressive; hence

$$\varepsilon^c_{dyn} = \begin{cases} 1.225 \times 10^{-5} N^{0.314} 10^{0.033\sigma_{dyn}}, & \text{if } \sigma_{prmax} < 0, \quad (7a) \\ 7.985 \times 10^{-7} N^{0.4113} \sigma_{dyn}^{1.9063} N^{-0.116 \log \sigma_{dyn}}, & \text{if } \sigma_{prmax} > 0, \quad (7b) \end{cases}$$

where N is the number of loading cycles, and σ_{dyn} the stress amplitude in MPa.

As the creep process developed, the stress levels in the structure changed. Hence, an incremental procedure was required, and incremental creep strains were calculated, using an appropriate time step (Fig. 2). The value of the time step was defined by the ratio of the creep strain increment permitted, and the elastic strain. This ratio had a maximal value of 0.05 and ensured that the creep strain increments were small relative to the elastic strains; hence

$$\frac{\Delta\varepsilon^c}{\varepsilon^{el}} \leqslant 0.05. \quad (8)$$

The creep strain increment was then used in the FE code to calculate the various three-dimensional creep strain components ($\Delta\varepsilon^c_{ij}$), using a flow rule, which identifies how the Von Mises stress is affected by the various stress components, according to

$$\Delta\varepsilon^c_{ij} = \Delta\varepsilon^c \frac{\partial\sigma_{vm}}{\partial\sigma_{ij}}. \quad (9)$$

Using the creep-determined strain components and the stiffness matrix of the model, a nodal force vector was calculated which was subtracted from the force vector already present. Then a new FE iteration was performed with the modified force vector. This procedure was repeated until the simulation had reached 1.7 million loading cycles, as also realized in the experiments.

RESULTS

The application of the compressive force on the taper resulted in its subsidence, and in the generation of tensile hoop strains in the cement mantle. A schematic representation of the subsidence pattern is shown in Fig. 4. When the load was reduced to zero again, the taper remained stuck in the cement mantle and did not return to its original position. In the subsequent loading cycles the taper subsided only marginally until suddenly it subsided with a relatively large step. This mechanism was repeated a number of times, resulting in stepwise subsidence of the taper within the cement mantle with a step frequency much lower than the loading frequency (Fig. 5). These phenomena were found in both experiments, although the steps were much smaller and the step frequency higher in the experiment with Taper 2 as compared to Taper 1. After 1.7 million loading cycles, Taper 1 had subsided 630 μm, whereas Taper 2 subsided 380 μm within the cement mantle.

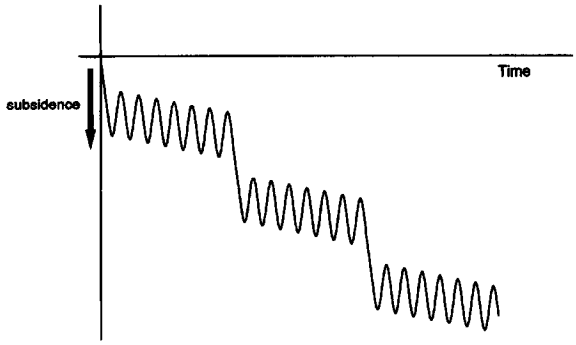

Fig. 4. A schematic representation of the subsidence pattern of the taper within the cement mantle. Initially, the taper subsided in the cement mantle, and did not return to its original position after unloading. In the subsequent loading cycles the taper subsided only marginally until suddenly the taper subsided with a relatively large step.

The stepwise subsidence pattern as found in the experiments was reproduced in the creep simulations, whereby the amount of subsidence depended largely on the value of the coefficient of friction at the taper–cement interface (Fig. 5). Increasing the coefficient of friction from 0.25 to 0.5 led to a reduction of about 25% in the maximal Von Mises stress levels. Due to the fact that the creep strains are very sensitive to small variations in the stress levels [see equations (5) and (7)], friction considerably affected the subsidence. Increasing the friction from 0.25 to 0.50 reduced the total subsidence and the step frequency by about 50%. Assuming friction coefficients of 0.25 and 0.5, subsidence patterns were predicted approximating those found in the two experiments.

The discontinuities in the subsidence patterns could be explained by stick–slip phenomena occurring at the taper–cement interface. Figure 6 depicts only a small part of the subsidence pattern, with the stick–slipping modes of the nodal points at the interface in the FE model. When the interface was completely in sticking mode, high cement stresses occurred in the tip region. As a result, the material crept primarily in this region, leading to a reduction of normal interface stress, and a reduction of the frictional force. The sticking mode was then transformed to a slipping one in this region. This process continued until the whole interface was in slipping mode, leading to a relatively large subsidence increment of the taper in the

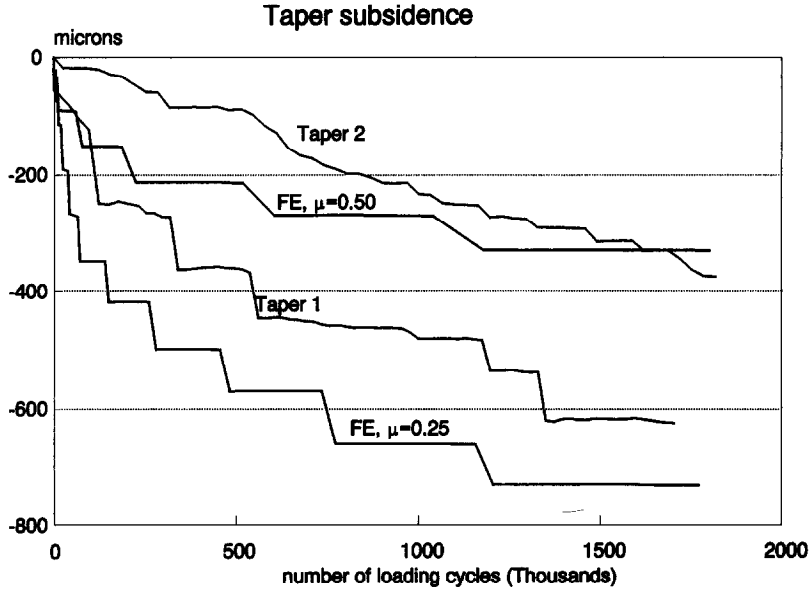

Fig. 5. The stepwise subsidence patterns were found in both experiments, although the discontinuities were much smaller, and occurred more frequently in the experiment with Taper 2. These patterns were reproduced in the creep simulations. A higher subsidence rate was found when taper–cement friction was reduced.

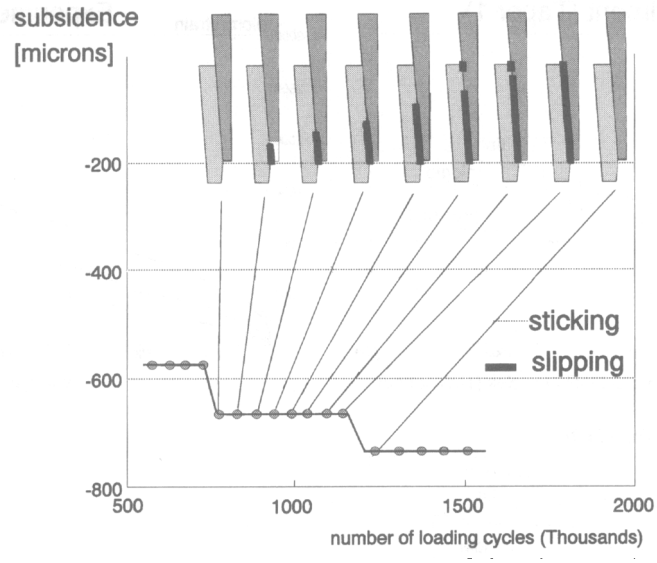

Fig. 6. The discontinuities in the subsidence patterns could be explained by stick–slip phenomena occurring at the taper–cement interface. When the interface is completely in sticking mode, high cement stresses occur in the tip region. Consequently, the material creeps in this region, and the sticking mode is transformed to a slipping one. This process continues until the whole interface is in slipping mode, leading to a relatively large subsidence increment.

cement mantle. After this point in time the process was repeated.

As the tapers subsided in the cement mantle, the hoop strains at the exterior of the cement mantle increased with the number of loading cycles. The creep strains generated around Taper 1 were consistently higher (about 20%) than those generated around Taper 2. Due to the fact that the tapers showed stepwise subsidence patterns, the increase of the strain values occurred also discontinuously. This phenomenon was also found in the FE creep simulations (Fig. 7). The stress levels in the tip region were higher than the proximal ones. This resulted in relatively high creep rates in the former region. Variation in friction from 0.25 to 0.50 reduced the creep hoop strains at the exterior of the cement mantle by about 30%.

DISCUSSION

In this study uniaxial creep properties of bone cement were implemented in an axisymmetrical FE model to analyze the mechanisms involved in prosthetic subsidence. Results were compared to those obtained with laboratory experiments. The use of the creep laws in the FE models is hampered by two problems; one concerns the multiaxial stress state apparent in the bone cement and the second concerns the stress characteristics, which are neither purely static nor purely dynamic. The first problem is quite common in creep simulations, and usually the Von Mises stress is used to generalize the multiaxial stress state to the uniaxial ones occurring in material creep tests. The second problem was solved by separating the Von Mises stress level into a static and dynamic one. Combinations of dynamic and static creep laws were then used at locations where the bone cement was loaded under a combination of dynamic and residual loads. This method introduces two uncertainties. First of all, the superposition of the static and dynamic creep-strain increments applied here, is based on Boltzmann's principle (Young and Lovell, 1991). This principle is valid for materials that are linear visco-elastic. Hand-mixed, radiopaque bone cement has a capricious material behavior, which is very sensitive to mixing procedures, additives and test conditions, and the application of Boltzmann's principle in this study implies an idealization of reality. A second factor of uncertainty is the ratio that determined which part of the Von Mises stress level was subject to the static creep law and which part to the dynamic ones. In every integration point, the ratio was determined prior to the actual creep simulation and was assumed to remain constant during the creep process. Hence, the static stress level as well as the dynamic stress amplitude were assumed to change likewise if the maximal stress level changed as a consequence of creep. Whether this is a realistic assumption was examined by calculating this ratio at the end of one creep simulation of 1.7 million loading cycles. It was found that prior to the creep simulation, the average residual stress was 63% of that generated at full loading. After the creep simulation, this percentage had increased to 70%. This means that the residual stress levels are higher and the dynamic ones are lower at the end-stage of the creep simulation than determined prior to the creep simulation. However, it is expected that this phenomenon will not cause large errors in the creep strain calculation as these two errors partly compensate each other.

The study showed that stem subsidence does occur due to creep of acrylic bone cement when loaded dynamically, and can be effectively analyzed with

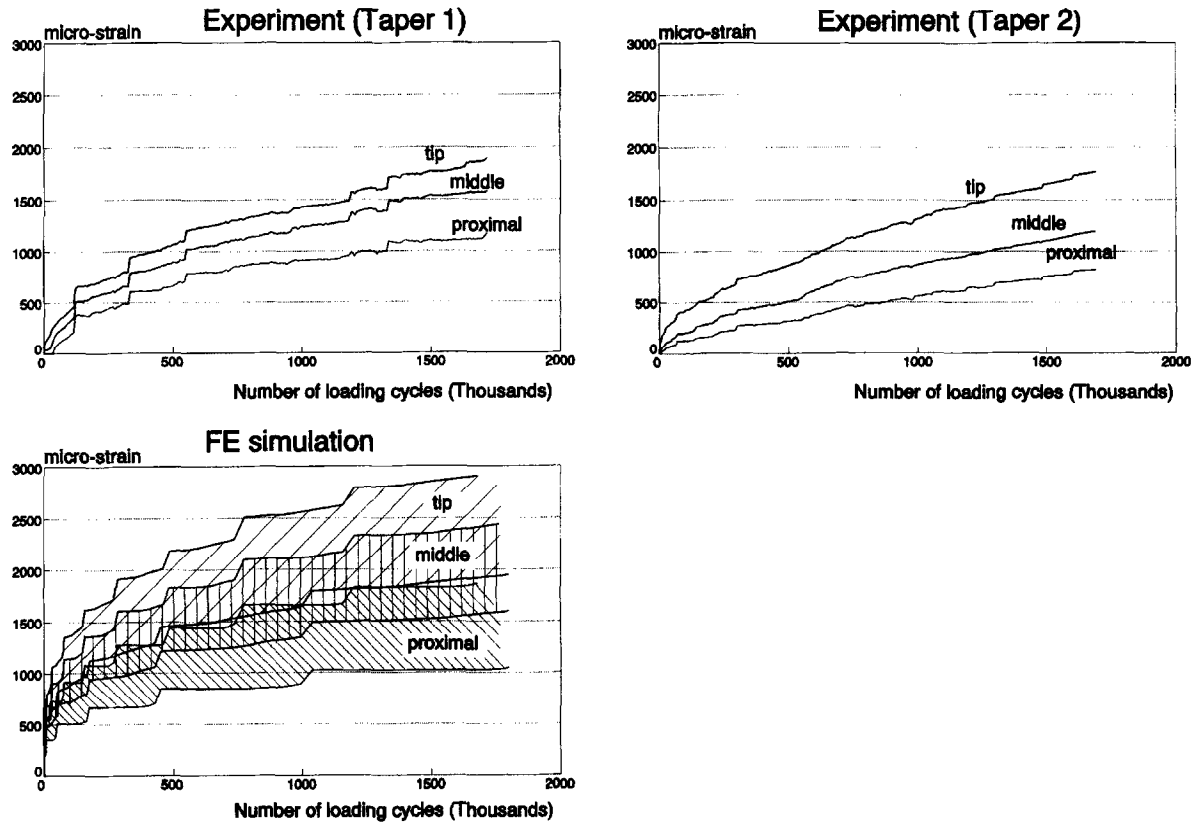

Fig. 7. As the taper subsided in the cement mantle, the hoop strains at the exterior of the cement mantle increased with the number of loading cycles. Due to the fact that the taper showed a stepwise subsidence, the increase of the strain values occurred also discontinuously. The dashed areas are FE results in case of coefficients of friction between 0.25 (upper boundary) and 0.5 (lower boundary).

FE-techniques. The subsidence was step-wise instead of continuous. This phenomenon was caused by stick–slip mechanisms at the interface, starting distally and gradually working towards proximal as demonstrated by the FE simulation. The rate of this process was considerably different in the two experiments, leading to a different step frequency and total subsidence. The surface roughness of the two tapers was almost identical, but the cement mantles were probably not, as they were produced with hand-mixed cement. This may have led to differences in bulk and interface cement porosity. This might explain the differences in total subsidence and step frequency observed in the experiments. In the FE simulations, a similar trend was found when friction at the interface was varied. A relatively small increase of friction led to a significant reduction in step frequency and total subsidence. The rate of the creep process decreases in time, indicating that although creep does continue for a very long time, it may become insignificant after a long-term period.

It should also be realized that the effects of creep in terms of subsidence and stress relaxation are considerably affected by prosthetic design features (prosthetic shape, ridges, collar/calcar contact, surface roughness, etc.). At this point in time, it is uncertain which prosthetic type optimally accommodates creep of acrylic cement. A tapered polished stem may subside and stabilize itself (Ling, 1992). However, cement creep will also occur around stems which firmly bond to the cement mantle, which may lead to relaxation of cement stresses (Harris, 1992).

The experimental and FE findings demonstrate that prosthetic subsidence is a process which is extremely sensitive to small variations in surface roughness and cement constitution. It is likely that variations in THA reconstructions in patients are larger than those in the present experiments. Large variations in the bulk and interface porosity in the cement can be expected. In their retrieval study, James *et al.* (1993) demonstrated that cement porosity at the stem–cement interface can be as high as 50%, and varies considerably among patients. Interface porosity not only reduces the effective surface area available for load-transfer, but also alters the stem–cement frictional properties, which will affect prosthetic subsidence as demonstrated in this study. These factors may explain the relatively large variation of *in vivo* prosthetic subsidence rates reported in the literature (Fowler *et al.*, 1988).

Acknowledgement—This work was partly supported by Howmedica Int., Staines, U.K.

REFERENCES

Ahmed, A. M., Nair, R., Burke, E. L. and Miller, J. E. (1982) Transient and residual stresses in self curing bone cement. Part II: Thermoelastic analysis of the stem fixation system. *J. Biomech. Engng* **104,** 28–37.

Chwirut, D. J. (1984) Long-term compressive creep deformation and damage in acrylic bone elements. *J. Biomed. Mater. Res.* **18,** 25–37.

Fowler, J. L., Gie, G. A., Lee, A. J. C. and Ling, R. S. M. (1988) Experience with the exeter total hip replacement since 1970. *Orthop. Clin. North Am.* **19,** 25–37.

Hampton, S. J. (1981) A nonlinear finite element model of adhesive bond failure and application to total hip replacement analysis. Ph.D. thesis, University of Illinois at Chicago Circle, Chicago, Illinois, pp. 81–86.

Harris, W. H. (1992) Is it advantageous to strengthen the cement–metal interface and use a collar for cemented femoral components of total hip replacement? *Clin. Orthop.* **285,** 67–72.

Hinton, E. (1992) NAFEMS Introduction to nonlinear finite element analysis. Bell and Bain Ltd., Glasgow, Great Britain.

James, S. P., Schmalzried, T. P., McGary, F. J. and Harris, W. H. (1993) Extensive porosity at the cement–femoral prosthesis interface: a preliminary study. *J. Biomed. Mater. Res.* **27,** 71–78.

Lee, A. J. C., Perkins, R. D. and Ling, R. S. M. (1990) Time-dependent properties of polymethylmethacrylate bone cement. In *Implant Bone Interface* (Edited by Older, J.), Ch. 12, pp. 85–90. Springer, Berlin.

Ling, R. S. M. (1992) The use of a collar and precoating on cemented femoral stems is unnecessary and detrimental. *Clin. Orthop.* **285,** 73–82.

Mann, K. A., Bartel, D. L., Wright, T. M. and Ingraffea, A. R. (1991) Mechanical characteristics of the stem–cement interface. *J. Orthop. Res.* **9,** 798–808.

Oysæed, H. and Ruyter, I. E. (1989) Creep studies of multiphase acrylic systems. *J. Biomed. Mater. Res.* **23,** 719–733.

Saha, S. and Pal, S. (1982) Stress relaxation and creep behavior of normal and carbon fibre reinforced acrylic bone cement. *Biomaterials* **3,** 93–96.

Saha, S. and Pal, S. (1984) Mechanical properties of bone cement: a review. *J. Biomed. Mater. Res.* **18,** 435–462.

Treharne, R. W. and Brown, N. (1975) Factors influencing the creep behavior of poly(methyl methacrylate) cements. *J. Biomed. Mater. Res.* **6,** 81–88.

Verdonschot, N. and Huiskes, R. (1994) The creep behavior of hand-mixed Simplex P bone cement under cyclic tensile loading. *J. Appl. Biomater.* **5,** 235–243.

Verdonschot, N. and Huiskes, R. (1995a) Dynamic creep behavior of acrylic bone cement. *J. Biomed. Mater. Res.* **29,** 575–581.

Verdonschot, N. and Huiskes, R. (1995b) The effect of stem–cement interface characteristics on the survival of femoral THR. *Clin. Orthop. Rel. Res.* (in press).

Young, R. J. and Lovell, P. A. (1991) *Introduction to Polymers.* The University Press, Cambridge, U.K.